


Effective-mass tensor of the two-body bound states and the quantum-metric tensor of the underlying Bloch states in multiband lattices

M. Iskin

Department of Physics, Koç University, Rumelifeneri Yolu, 34450 Sarıyer, Istanbul, Turkey
 (Received 12 September 2021; accepted 25 January 2022; published 9 February 2022; corrected 24 May 2022)

By considering an on-site attraction between a spin- \uparrow and a spin- \downarrow fermion in a multiband tight-binding lattice, here we study the two-body spectrum and derive an exact relation between the inverse of the effective-mass tensor of the lowest bound states and the quantum-metric tensor of the underlying Bloch states. In addition to the intraband (or the so-called conventional) contribution that depends only on the single-particle spectrum and the interband (or the so-called geometric) contribution that is controlled by the quantum metric, our generalized relation has an additional interband contribution that depends on the so-called band-resolved quantum metric. All of our analytical expressions are applicable to those multiband lattices that simultaneously exhibit time-reversal symmetry and fulfill the condition on spatially uniform pairing. As a nontrivial illustration we analyze the two-body problem in a kagome lattice with nearest-neighbor hoppings, and we show that the exact relation provides a perfect benchmark.

DOI: [10.1103/PhysRevA.105.023312](https://doi.org/10.1103/PhysRevA.105.023312)

I. INTRODUCTION

The quantum-metric tensor is defined as the real part of the quantum-geometric tensor (whose imaginary part is the Berry curvature), and in condensed-matter physics it provides a measure of the so-called quantum distance between the nearby Bloch states in momentum space [1–3]. Together with the Berry curvature, it constitutes one of the two band-structure invariants that have gradually become central objects in a number of fields. For instance, the quantum metric plays a crucial role in the transport properties of some multiband superfluids and superconductors: it controls the effective-mass tensor of the superfluid carriers through the interband processes, which in return affects all of the other superfluid properties that depend on the carrier mass including, e.g., the superfluid weight and density, the velocity of the low-energy collective modes such as the Goldstone mode, the Berezinskii-Kosterlitz-Thouless transition temperature, etc. [4–11]. Given these theoretical predictions and many others, there has been rapid progress and a growing demand for measuring the quantum metric itself [12–16].

In connection to the central theme of this paper, we have recently derived a Ginzburg-Landau functional for a spin-orbit-coupled Fermi superfluid in continuous space [within the BCS-BEC (Bose-Einstein condensate) mean-field theory and Gaussian fluctuations on top of it] and revealed a direct relation between the inverse of the effective-mass tensor of the many-body bound states (e.g., Cooper pairs) and the quantum-metric tensor of the helicity states [7]. See also Ref. [8]. Then, by assuming a sufficiently weak on-site attraction between the particles in a multiband lattice, a parallel relation has been derived for the two-body bound states in vacuum by focusing on an isolated flat band that is separated from the remaining ones with a finite band gap [17]. More recently, by assuming an

on-site attraction and time-reversal symmetry, we have found an analogous but exact relation for the effective-mass tensor of the lowest bound states in generic two-band lattices [18]. In this paper we extend and generalize the latter study to multiband lattices and show that in addition to the intraband (or the so-called conventional) contribution that depends only on the single-particle spectrum and the interband (or the so-called geometric) contribution that is controlled by the quantum metric, there is an additional interband contribution that depends on the so-called band-resolved quantum metric. The revelation of the latter contribution is one of our main results in this work. All of our analytical expressions are applicable to a certain class of multiband lattices that simultaneously exhibit time-reversal symmetry and fulfill the condition on spatially uniform pairing, i.e., when the two-body wave function is uniformly delocalized over the sublattices. This is expected to be the case for those Bloch Hamiltonians that are invariant under the interchange of their sublattices. Furthermore, we show that our general relation reproduces all of the known results in the respective limits, and it is in perfect agreement with the exact solution to the two-body problem in a kagome lattice with nearest-neighbor hoppings.

The rest of the paper is organized as follows. First we study the kagome model in Sec. II: the single-particle band structure is reviewed in Sec. II A and the two-body spectrum is analyzed in Sec. II B. Then we relate our numerical findings to the quantum metric in Sec. III and discuss the versatility of our results for other lattices in Sec. IV. The paper ends with a brief summary of conclusions and an outlook given in Sec. V.

II. KAGOME LATTICE

As a physical motivation for the exact relation between the inverse of the effective-mass tensor of the lowest two-body

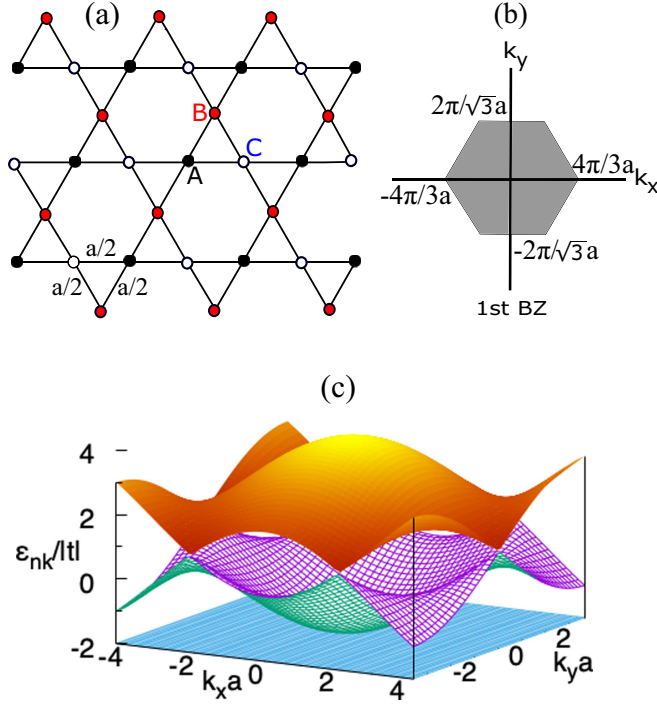


FIG. 1. Sketches of (a) the crystal structure in real space and (b) the first Brillouin zone in reciprocal space. (c) Band structure with a flat band at the bottom. Note that while the flat band is in quadratic touch with a dispersive band at the origin, the dispersive bands touch each other and form Dirac cones at the six corners of the Brillouin zone.

bound states and the quantum-metric tensor of the underlying Bloch states, here we want to analyze a nontrivial yet analytically tractable multiband tight-binding lattice that features a flat band in its band structure. Given their recent realizations, kagome [19–22] and Lieb [23–25] lattices are probably the ideal candidates, and here we focus on the former model with nearest-neighbor hopping.

A. Band structure

The kagome crystal structure with nearest-neighbor bonds is illustrated in Fig. 1(a): it forms a triangular lattice with a side length a and has a three-point ($N_b = 3$) basis that is located at $\mathbf{r}_A = (0, 0)$, $\mathbf{r}_B = \frac{a}{4}(1, \sqrt{3})$, and $\mathbf{r}_C = \frac{a}{2}(1, 0)$. The real-space primitive unit vectors can be chosen as $\mathbf{a}_1 = a(1, 0)$ and $\mathbf{a}_2 = \frac{a}{2}(1, \sqrt{3})$, and we define $\mathbf{a}_3 = \mathbf{a}_1 - \mathbf{a}_2$ for convenience. If the entire lattice is constructed with N_c unit cells then the total number of lattice sites is $N = N_b N_c$. Accordingly the reciprocal-space primitive unit vectors can be chosen as $\mathbf{b}_1 = \frac{2\pi}{\sqrt{3}a}(\sqrt{3}, -1)$ and $\mathbf{b}_2 = \frac{4\pi}{\sqrt{3}a}(0, 1)$, and they satisfy $\mathbf{a}_i \cdot \mathbf{b}_j = 2\pi \delta_{ij}$ with δ_{ij} being the Kronecker delta. The corresponding first Brillouin zone is illustrated in Fig. 1(b) whose area is $8\pi^2/(\sqrt{3}a^2)$. This is in such a way that the Brillouin zone contains a total of $\sum_{\mathbf{k}} 1 = N_c$ distinct \mathbf{k} -space points.

The Hamiltonian for a single spin- $\sigma = \{\uparrow, \downarrow\}$ particle can be written as $\mathcal{H}_\sigma = \sum_{\mathbf{k}} \psi_{\mathbf{k}\sigma}^\dagger \mathbf{H}_{\mathbf{k}\sigma} \psi_{\mathbf{k}\sigma}$, where $\psi_{\mathbf{k}\sigma} = (c_{A\mathbf{k}\sigma} \ c_{B\mathbf{k}\sigma} \ c_{C\mathbf{k}\sigma})^T$ is a three-component spinor with T being the transpose operator and $c_{S\mathbf{k}\sigma}$ the annihilation operator for a spin- σ particle on the sublattice S with a crystal momentum

$\mathbf{k} = (k_x, k_y)$. In the orbital basis $|S\mathbf{k}\sigma\rangle = c_{S\mathbf{k}\sigma}^\dagger |0\rangle$ with $|0\rangle$ being the vacuum state, the Hamiltonian density can be written as

$$\mathbf{H}_{\mathbf{k}\sigma} = -2t \begin{bmatrix} 0 & \cos\left(\frac{\mathbf{k}\cdot\mathbf{a}_2}{2}\right) & \cos\left(\frac{\mathbf{k}\cdot\mathbf{a}_1}{2}\right) \\ \cos\left(\frac{\mathbf{k}\cdot\mathbf{a}_2}{2}\right) & 0 & \cos\left(\frac{\mathbf{k}\cdot\mathbf{a}_3}{2}\right) \\ \cos\left(\frac{\mathbf{k}\cdot\mathbf{a}_1}{2}\right) & \cos\left(\frac{\mathbf{k}\cdot\mathbf{a}_3}{2}\right) & 0 \end{bmatrix}, \quad (1)$$

where t is the hopping element between the nearest-neighbor lattice sites. The single-particle spectrum $\varepsilon_{n\mathbf{k}\sigma}$ is given by the eigenvalues of $\mathbf{H}_{\mathbf{k}\sigma}$, leading to [26,27]

$$\varepsilon_{1\mathbf{k}\sigma} = 2t, \quad (2)$$

$$\varepsilon_{2\mathbf{k}\sigma} = -t - |t|\sqrt{2\Lambda_{\mathbf{k}} + 3}, \quad (3)$$

$$\varepsilon_{3\mathbf{k}\sigma} = -t + |t|\sqrt{2\Lambda_{\mathbf{k}} + 3}, \quad (4)$$

which are independent of the spin of the particle. Here the first band is flat and nondispersive in \mathbf{k} space, and the dispersive bands are characterized by $\Lambda_{\mathbf{k}} = \sum_{i=1}^3 \cos(\mathbf{k} \cdot \mathbf{a}_i)$. We choose a negative $t = -|t|$ in this paper leading to a flat band at the bottom. The resultant band structure is shown in Fig. 1(c). We note that, while the flat band is in quadratic touch with a dispersive band at $\mathbf{k} = \mathbf{0}$, the dispersive bands touch each other and form Dirac cones at the six corners of the Brillouin zone.

Given our interest in the dispersion of the two-body bound states, we need not only the band structure but also the associated Bloch states $|n\mathbf{k}\sigma\rangle$. Thus, a compact way to express the eigenvectors of $\mathbf{H}_{\mathbf{k}\sigma}$ is [26,27]

$$|1\mathbf{k}\sigma\rangle \equiv \begin{pmatrix} 1_{A\mathbf{k}\sigma} \\ 1_{B\mathbf{k}\sigma} \\ 1_{C\mathbf{k}\sigma} \end{pmatrix} = \mathcal{A}_{1\mathbf{k}} \begin{bmatrix} \sin(\theta_{2\mathbf{k}} - \theta_{3\mathbf{k}}) \\ \sin(\theta_{3\mathbf{k}} - \theta_{1\mathbf{k}}) \\ \sin(\theta_{1\mathbf{k}} - \theta_{2\mathbf{k}}) \end{bmatrix}, \quad (5)$$

$$|2\mathbf{k}\sigma\rangle \equiv \begin{pmatrix} 2_{A\mathbf{k}\sigma} \\ 2_{B\mathbf{k}\sigma} \\ 2_{C\mathbf{k}\sigma} \end{pmatrix} = \mathcal{A}_{2\mathbf{k}} \begin{bmatrix} \sin(\theta_{1\mathbf{k}} + \phi_{\mathbf{k}}) \\ \sin(\theta_{2\mathbf{k}} + \phi_{\mathbf{k}}) \\ \sin(\theta_{3\mathbf{k}} + \phi_{\mathbf{k}}) \end{bmatrix}, \quad (6)$$

$$|3\mathbf{k}\sigma\rangle \equiv \begin{pmatrix} 3_{A\mathbf{k}\sigma} \\ 3_{B\mathbf{k}\sigma} \\ 3_{C\mathbf{k}\sigma} \end{pmatrix} = \mathcal{A}_{3\mathbf{k}} \begin{bmatrix} \cos(\theta_{1\mathbf{k}} + \phi_{\mathbf{k}}) \\ \cos(\theta_{2\mathbf{k}} + \phi_{\mathbf{k}}) \\ \cos(\theta_{3\mathbf{k}} + \phi_{\mathbf{k}}) \end{bmatrix}, \quad (7)$$

where $n_{S\mathbf{k}\sigma} = \langle S|n\mathbf{k}\sigma\rangle$ is the projection of the Bloch state onto the S th sublattice; $\mathcal{A}_{n\mathbf{k}}$ is the normalization factor; and $\theta_{1\mathbf{k}} = k_x a/4 + k_y a/(4\sqrt{3})$, $\theta_{2\mathbf{k}} = -k_y a/(2\sqrt{3})$, $\theta_{3\mathbf{k}} = -k_x a/4 + k_y a/(4\sqrt{3})$, and $\phi_{\mathbf{k}} = \frac{1}{2} \arg[e^{ik_y a/\sqrt{3}} + 2 \cos(k_x a/2) e^{-ik_x/(2\sqrt{3})}]$ are some phase factors associated with the geometry of the kagome lattice. Having completed the analysis of the one-body problem, next we proceed with the two-body problem.

B. Two-body bound states

In the presence of a multiband tight-binding lattice, it is possible to solve the two-body problem exactly through a variational approach that is based on the following ansatz [18]:

$$|\Psi_{\mathbf{q}}\rangle = \sum_{nm\mathbf{k}} \alpha_{nm\mathbf{k}}^{\mathbf{q}} c_{n,\mathbf{k}+\mathbf{q}/2,\uparrow}^\dagger c_{m,-\mathbf{k}+\mathbf{q}/2,\downarrow}^\dagger |0\rangle. \quad (8)$$

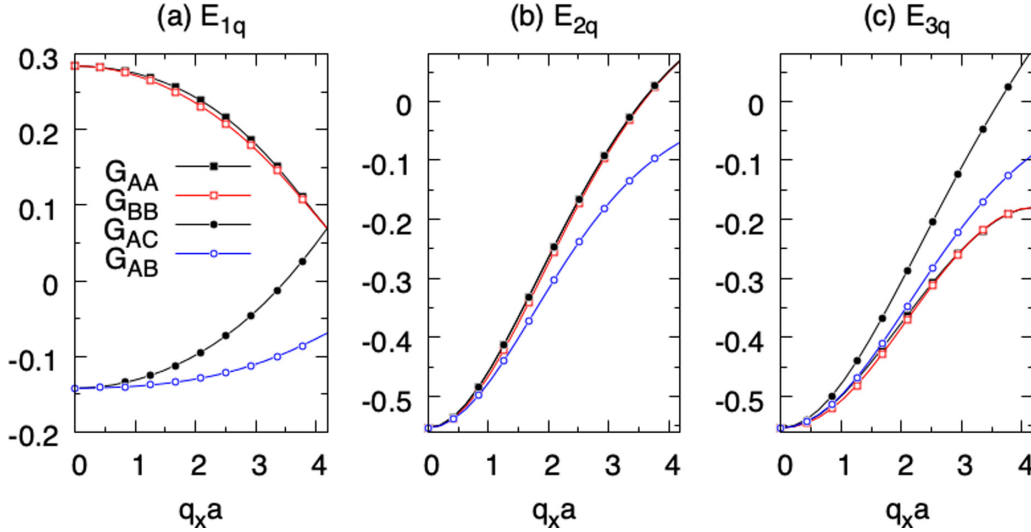


FIG. 2. Matrix elements $G_{SS'}^q$ for $U = 2|t|$ as a function of q_x when $q_y = 0$. Here panels (a), (b), and (c) correspond, respectively, to the self-consistent solutions for E_{1q} , E_{2q} , and E_{3q} . Since $G_{CC}^q = G_{AA}^q$ and $G_{BC}^q = G_{AB}^q$ for all q_x , these coefficients are not shown. Note that $G_{AA}^q = G_{BB}^q$ and $G_{AB}^q = G_{AC}^q$ in the small- $q_x a$ limit. In addition, together with the characteristic (bound state) Eq. (9), these coefficients imply $\beta_{1q} \propto (1, 1, 1)$, $\beta_{2q} \propto (1, 0, -1)$, and $\beta_{3q} \propto (1, -2, 1)$ in the small- $q_x a$ limit.

Here \mathbf{q} is the center-of-mass momentum of the spin-singlet bound pair that is formed between a spin- \uparrow and a spin- \downarrow particle, the variational parameter $\alpha_{nm\mathbf{k}}^q$ is a complex number in general, and the operator $c_{nk\sigma}^\dagger$ creates a particle in the Bloch state $|n\mathbf{k}\sigma\rangle = c_{nk\sigma}^\dagger|0\rangle$. The creation operators in the orbital and Bloch basis are related through $c_{nk\sigma}^\dagger = \sum_S n_{S\mathbf{k}\sigma} c_{S\mathbf{k}\sigma}^\dagger$ since $\sum_S |S\mathbf{k}\sigma\rangle\langle S\mathbf{k}\sigma| = \mathcal{I}_{N_b}$ is an identity operator in N_b dimensions for a given \mathbf{k} and σ . The dispersion $E_{\ell\mathbf{q}}$ of the bound state is determined through the minimization of $\langle\Psi_{\mathbf{q}}|\mathcal{H} - E_{\ell\mathbf{q}}|\Psi_{\mathbf{q}}\rangle = 0$ with respect to $\alpha_{nm\mathbf{k}}^q$, where $\mathcal{H} = \mathcal{H}_\uparrow + \mathcal{H}_\downarrow + \mathcal{H}_{\uparrow\downarrow}$ is the total Hamiltonian of the system. Here we limit our analysis to an on-site (i.e., contact) attraction between the particles thanks mainly to the clarity of the central theme of this paper. For this purpose let us consider $\mathcal{H}_{\uparrow\downarrow} = -U \sum_{Si} \rho_{Si\uparrow} \rho_{Si\downarrow}$, where $U \geq 0$ is the strength of the interaction and $\rho_{Si\sigma} = c_{Si\sigma}^\dagger c_{Si\sigma}$ is the number operator at the S th sublattice in the i th unit cell. Here the operator $c_{Si\sigma}$ corresponds to the Fourier transform of $c_{S\mathbf{k}\sigma}$. In addition, we take advantage of the time-reversal symmetry and set $n_{S\mathbf{k}\uparrow} = n_{S,-\mathbf{k},\downarrow}^* \equiv n_{S\mathbf{k}}$ and $\varepsilon_{n\mathbf{k}\uparrow} = \varepsilon_{n,-\mathbf{k},\downarrow} \equiv \varepsilon_{n\mathbf{k}}$. After some straightforward algebra [18], $E_{\ell\mathbf{q}}$ is characterized by a set of linear equations,

$$\mathbf{G}^q \boldsymbol{\beta}_{\ell\mathbf{q}} = 0, \quad (9)$$

where \mathbf{G}^q is an N_b -dimensional Hermitian matrix with the following elements:

$$G_{SS'}^q = \delta_{SS'} - \frac{U}{N_c} \sum_{nm\mathbf{k}} \frac{m_{S\mathbf{K}}^* n_{S\mathbf{K}} n_{S'\mathbf{K}'}^* m_{S'\mathbf{K}'}}{\varepsilon_{n\mathbf{K}} + \varepsilon_{m\mathbf{K}'} - E_{\ell\mathbf{q}}}. \quad (10)$$

Here $\mathbf{K} = \mathbf{k} + \mathbf{q}/2$ and $\mathbf{K}' = \mathbf{k} - \mathbf{q}/2$. Thus, $E_{\ell\mathbf{q}}$ is determined by setting $\det \mathbf{G}^q = 0$, and there are N_b solutions for a given \mathbf{q} . We label these solutions with $\ell = \{1, 2, 3\}$ starting from the lower branch. Furthermore, the state vector $\boldsymbol{\beta}_{\ell\mathbf{q}} = (\beta_{A\ell\mathbf{q}} \beta_{B\ell\mathbf{q}} \beta_{C\ell\mathbf{q}})^T$, where $\beta_{S\ell\mathbf{q}} = \sum_{nm\mathbf{k}} \alpha_{nm\mathbf{k}}^q n_{S\mathbf{K}} m_{S'\mathbf{K}'}$ is the corresponding eigenvector of \mathbf{G}^q , and it carries further insight into the physical mechanism and nature of the bound state.

Our numerical calculations for the kagome lattice show that the matrix elements of \mathbf{G}^q have the following properties. When \mathbf{q} is along one of the principal axis, i.e., either when $q_x = 0$ or $q_y = 0$, we observe that $G_{AA}^q = G_{CC}^q$ and $G_{AB}^q = G_{BC}^q$ for all parameters. Thus, one of the eigenvalues of $\mathbf{G}^q = 0$ is $G_{AA}^q - G_{AC}^q$ with the eigenvector $\beta_{2q} \propto (1, 0, -1)$, and it determines the middle branch E_{2q} . The upper branch E_{3q} and the lower one E_{1q} are determined, respectively, by the eigenvalues $(G_{AA}^q + G_{BB}^q + G_{AC}^q)/2 \pm [8(G_{AA}^q)^2 + (G_{AC}^q)^2 + (G_{AA}^q - G_{BB}^q)(2G_{AC}^q + G_{AA}^q - G_{BB}^q)]^{1/2}/2$, where $\beta_{3q} \propto (1, Q_q, 1)$ with $Q_q < 0$ and $\beta_{1q} \propto (1, R_q, 1)$ with $R_q > 0$. While the \mathbf{q} dependencies of Q_q and R_q are not very illuminating and skipped, they are in such a way that $Q_q R_q = -2$ for every \mathbf{q} which is required by the orthonormalization of $\boldsymbol{\beta}_{\ell\mathbf{q}}$. Thus, by setting the eigenvalues of \mathbf{G}^q to 0, we find that E_{2q} is determined by the condition $G_{AA}^q = G_{AC}^q$ and that E_{1q} and E_{3q} are determined by the same condition $2(G_{AB}^q)^2 = G_{BB}^q (G_{AA}^q + G_{AC}^q)$. On the other hand, when $q = \sqrt{q_x^2 + q_y^2}$ is small, i.e., when $qa \ll 1$, we observe that $G_{AA}^q = G_{BB}^q = G_{CC}^q$ and $G_{AB}^q = G_{BC}^q = G_{AC}^q$ for all parameters. These are shown in Fig. 2. Thus E_{1q} is determined by the condition $G_{AA}^q = -2G_{AB}^q$, and it is characterized by $\beta_{1q} \propto (1, 1, 1)$. This suggests that the low-energy bound states can be distinguished by their perfectly in-phase (i.e., spatially uniform) contribution from all three sublattices [28]. On the other hand E_{2q} and E_{3q} are both determined by the very same condition $G_{AA}^q = G_{AB}^q$ (i.e., they are degenerate in the small- q limit) and are characterized, respectively, by $\beta_{2q} \propto (1, 0, -1)$ and $\beta_{3q} \propto (1, -2, 1)$.

As an illustration we set $U = 2|t|$ and $q_y = 0$ in Fig. 3(a) and present the two-body spectrum $E_{\ell\mathbf{q}}$ as a function of q_x . Even though E_{3q} disperses in \mathbf{q} , it appears quite flat and featureless in the presented scale. We observe that while E_{3q} and E_{2q} are degenerate at low q , E_{2q} and E_{1q} are degenerate at the corner of the Brillouin zone. More importantly the quadratic expansion of $E_{1q} = E_b + q^2/(2M_b)$ provides an

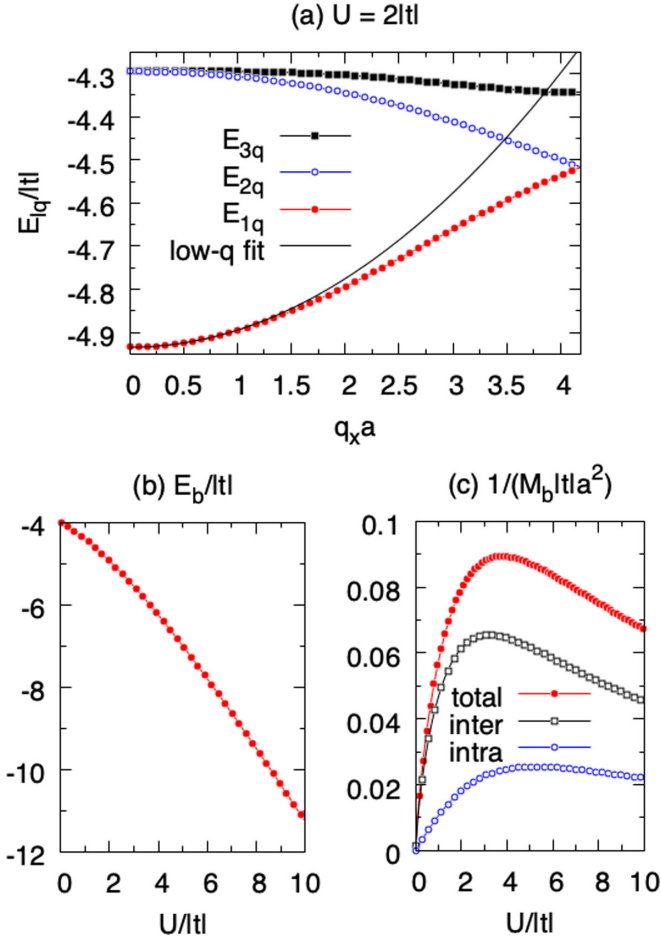


FIG. 3. (a) Two-body spectrum E_{lq} for $U = 2|t|$ as a function of q_x when $q_y = 0$. The quadratic expansion of $E_{1q} = E_b + q^2/(2M_b)$ is an excellent fit for the lower branch in the small- q limit. (b) E_b as a function of U . (c) $1/M_b = 1/M_b^{\text{intra}} + 1/M_b^{\text{inter}}$ as a function of U along with its intraband and interband contributions, where $1/M_b^{\text{inter}} = 1/M_b^{\text{inter},1} + 1/M_b^{\text{inter},2}$.

excellent fit for the lower branch in the small- q limit, where $E_b \approx -4.934|t|$ is the energy of the lowest bound state and $M_b \approx 12.574/(|t|a^2)$ is its effective mass. We remark here that the effective masses of the E_{1q} and E_{2q} branches become very close to each other (in magnitude) as U gets larger and larger. In order to gain deeper insight into the former result, next we use our observation that $\beta_{1q} \propto (1, 1, 1)$ for the lower band in the small- q limit. Furthermore this observation allows us to derive the generalized relation between the inverse of the effective-mass tensor of the lowest bound states and the quantum-metric tensor of the underlying Bloch states for those multiband lattices that simultaneously exhibit time-reversal symmetry and fulfill the condition on spatially uniform pairing.

III. RELATION TO QUANTUM METRIC

Given our numerical observation that the small- q limit of the lower branch E_{1q} is characterized by $\beta_{1q} \propto (1, 1, 1)$, it is possible to isolate the condition that determines E_{1q} as $\sum_{SS'} G_{SS'}^q = 0$. This is a very convenient form, and it may

find practical applications in other multiband lattices as long as the lowest bound states are distinguished by a perfectly in-phase contribution from all of the sublattices, i.e., $\beta_{1q} \propto (1, 1, \dots, 1)$. Hoping that this is generically the case in time-reversal-symmetric systems with a spatially uniform pairing, below we keep the formalism and the discussion general. By plugging Eq. (10) into this condition, and observing that $\sum_S m_{S\mathbf{K}}^* n_{S\mathbf{K}} = \langle m_{\mathbf{K}'} | n_{\mathbf{K}} \rangle$ with $|n_{\mathbf{K}}\rangle$ representing the Bloch states that are given in Eqs. (5)–(7), we obtain a much simpler condition:

$$1 = \frac{U}{N} \sum_{nm\mathbf{k}} \frac{|\langle m_{\mathbf{k}-q/2} | n_{\mathbf{k}+q/2} \rangle|^2}{\varepsilon_{n,\mathbf{k}+q/2} + \varepsilon_{m,\mathbf{k}-q/2} - E_{1q}}. \quad (11)$$

Here $N = N_b N_c$ is the total number of lattice sites in the system. This expression can be used to make further analytical progress by taking its small- q limit.

For instance, in the presence of an energetically isolated flat band $\varepsilon_{f\mathbf{k}} = \varepsilon_f$ that is separated from the remaining bands with a finite band gap, Eq. (11) can be approximated by $1 = (U/N) \sum_{\mathbf{k}} |\langle f_{\mathbf{k}-q/2} | f_{\mathbf{k}+q/2} \rangle|^2 / (2\varepsilon_f - E_{1q})$ in the small- U limit, leading to [17] $E_{1q} = 2\varepsilon_f - (U/N) \sum_{\mathbf{k}} |\langle f_{\mathbf{k}-q/2} | f_{\mathbf{k}+q/2} \rangle|^2$. Furthermore, we use the Taylor expansions $|f_{\mathbf{k}\pm q/2}\rangle = |f_{\mathbf{k}} \pm (1/2) \sum_i q_i \partial_i f_{\mathbf{k}} + (1/8) \sum_{ij} q_i q_j \partial_i \partial_j f_{\mathbf{k}}\rangle$ in small \mathbf{q} and obtain $|\langle f_{\mathbf{k}-q/2} | f_{\mathbf{k}+q/2} \rangle|^2 = 1 - (1/2) \sum_{ij} q_i q_j g_{ij}^{f\mathbf{k}}$. This is exact up to second order in \mathbf{q} where $g_{ij}^{n\mathbf{k}} = \text{Tr}(\partial_i P_{n\mathbf{k}} \partial_j P_{n\mathbf{k}})$ is the matrix element of the so-called quantum-metric tensor of the Bloch state $|n_{\mathbf{k}}\rangle$ [3]. Here Tr is the trace, $\partial_i = \partial/\partial k_i$ is the partial derivative, and $P_{n\mathbf{k}} = |n_{\mathbf{k}}\rangle \langle n_{\mathbf{k}}|$ is the projection operator. Since $P_{n\mathbf{k}}$ is a gauge-independent operator by definition, $g_{ij}^{n\mathbf{k}}$ is also a band invariant. By noting that $\langle n_{\mathbf{k}} | \partial_i n_{\mathbf{k}} \rangle = -\langle \partial_i n_{\mathbf{k}} | n_{\mathbf{k}} \rangle$ is an imaginary number due to the normalization $\langle n_{\mathbf{k}} | n_{\mathbf{k}} \rangle = 1$ of the Bloch states, the quantum metric can be reexpressed in a more familiar form [1–3]:

$$g_{ij}^{n\mathbf{k}} = 2\text{Re} \langle \partial_i n_{\mathbf{k}} | (\mathcal{I}_{N_b} - |n_{\mathbf{k}}\rangle \langle n_{\mathbf{k}}|) \partial_j n_{\mathbf{k}} \rangle, \quad (12)$$

where Re is the real part of the expression. As a result we eventually find (i.e., to the lowest order in \mathbf{q})

$$E_{1q} = E_b + \frac{1}{2} \sum_{ij} q_i q_j (M_b^{-1})_{ij}, \quad (13)$$

where $E_b = 2\varepsilon_f - U/N_b$ is the threshold energy and $(M_b^{-1})_{ij} = (U/N) \sum_{\mathbf{k}} g_{ij}^{f\mathbf{k}}$ is the matrix element of the inverse of the effective-mass tensor \mathbf{M}_b . We remark here that these expressions are strictly valid in the small- U limit assuming an energetically isolated flat band [17].

Similarly one can perform a small- \mathbf{q} expansion of Eq. (11) and generalize E_b and \mathbf{M}_b^{-1} not only to arbitrary U values but also to arbitrary band structures. For this purpose we first use the Taylor expansions of $|n_{\mathbf{k}\pm q/2}\rangle$ given above and find $\langle m_{\mathbf{k}-q/2} | n_{\mathbf{k}+q/2} \rangle = \delta_{mn} + \sum_i q_i \langle m_{\mathbf{k}} | \partial_i n_{\mathbf{k}} \rangle - (1/8) \sum_{ij} q_i q_j (3\langle \partial_i m_{\mathbf{k}} | \partial_j n_{\mathbf{k}} \rangle + \langle \partial_j m_{\mathbf{k}} | \partial_i n_{\mathbf{k}} \rangle)$, where $\langle m_{\mathbf{k}} | n_{\mathbf{k}} \rangle = \delta_{mn}$ is due to the orthonormalization of the Bloch states and $\langle m_{\mathbf{k}} | \partial_i n_{\mathbf{k}} \rangle = -\langle \partial_i m_{\mathbf{k}} | n_{\mathbf{k}} \rangle$. This leads to $|\langle m_{\mathbf{k}-q/2} | n_{\mathbf{k}+q/2} \rangle|^2 = \delta_{mn} - \text{Re} \sum_{ij} q_i q_j \langle \partial_i n_{\mathbf{k}} | (\delta_{mn} - |m_{\mathbf{k}}\rangle \langle m_{\mathbf{k}}|) \partial_j n_{\mathbf{k}} \rangle$ in the small- \mathbf{q} limit. Then we expand the single-particle spectrum $\varepsilon_{n,\mathbf{k}\pm q/2} = \varepsilon_{n\mathbf{k}} \pm (1/2) \sum_i q_i \partial_i \varepsilon_{n\mathbf{k}} + (1/8) \sum_{ij} q_i q_j \partial_i \partial_j \varepsilon_{n\mathbf{k}}$ up to second order in \mathbf{q} and plug

Eq. (13) in Eq. (12) for the dispersion of the lowest bound states. By matching the coefficient of the zeroth-order terms in Eq. (11), we find

$$1 = \frac{U}{N} \sum_{nk} \frac{1}{2\varepsilon_{nk} - E_b}, \quad (14)$$

which is the self-consistency relation for the energy E_b of the lowest bound state. The first-order terms already vanish. By requiring that the second-order terms vanish, we find a closed-form expression for $\mathbf{M}_b^{-1} = \mathbf{M}_{\text{intra}}^{-1} + \mathbf{M}_{\text{inter}}^{-1}$, where $\mathbf{M}_{\text{intra}}^{-1}$ is the so-called conventional or the intraband contribution and $\mathbf{M}_{\text{inter}}^{-1} = \mathbf{M}_{\text{inter},1}^{-1} + \mathbf{M}_{\text{inter},2}^{-1}$ is the so-called geometric or the interband contribution to the inverse of the effective-mass tensor. They can be written as

$$(M_{\text{intra}}^{-1})_{ij} = \frac{1}{2D} \sum_{nk} \frac{\partial_i \partial_j \varepsilon_{nk}}{(2\varepsilon_{nk} - E_b)^2}, \quad (15)$$

$$(M_{\text{inter},1}^{-1})_{ij} = \frac{1}{D} \sum_{nk} \frac{g_{ij}^{nk}}{2\varepsilon_{nk} - E_b}, \quad (16)$$

$$(M_{\text{inter},2}^{-1})_{ij} = -\frac{1}{D} \sum_{n,m \neq n,k} \frac{g_{ij}^{nmk}}{\varepsilon_{nk} + \varepsilon_{mk} - E_b}, \quad (17)$$

where $D = \sum_{nk} \frac{1}{(2\varepsilon_{nk} - E_b)^2}$ and E_b is determined by Eq. (14) for a given U . Here Eq. (17) depends on the so-called band-resolved quantum metric

$$g_{ij}^{nmk} = 2\text{Re}\langle \partial_i n_{\mathbf{k}} | m_{\mathbf{k}} \rangle \langle m_{\mathbf{k}} | \partial_j n_{\mathbf{k}} \rangle, \quad (18)$$

since it produces the quantum metric of the n th band when summed over the rest of the bands, i.e., $g_{ij}^{nk} = \sum_{m \neq n} g_{ij}^{nmk}$. Equations (15)–(17) constitute the generalized relation between the inverse of the effective-mass tensor of the lowest bound states and the quantum-metric tensor of the underlying Bloch states, and they are exact.

Let us now reproduce the known results using Eqs. (14)–(17). In the case of an energetically isolated flat band $\varepsilon_{f\mathbf{k}} = \varepsilon_f$ that is separated from the remaining bands with a finite band gap, Eqs. (15) and (17) are negligible in the small- U limit. Furthermore Eq. (16) is approximated by $(M_{\text{inter},1}^{-1})_{ij} = (U/N) \sum_{\mathbf{k}} g_{ij}^{f\mathbf{k}}$ in the small- U limit, where $2\varepsilon_f - E_b = U/N_b$. These are in full agreement with the literature [17] and the discussion given below Eq. (11). On the other hand, in the case of a two-band ($N_b = 2$) lattice that is described by the Hamiltonian density $H_{\mathbf{k}\sigma} = d_0^{\mathbf{k}} \mathcal{I}_2 + \mathbf{d}_{\mathbf{k}} \cdot \boldsymbol{\tau}$ the single-particle spectrum is given by $\varepsilon_{s\mathbf{k}} = d_0^{\mathbf{k}} + s d_{\mathbf{k}}$, where $s = \{+, -\}$ labels, respectively, the upper and lower bands. Here $\boldsymbol{\tau} = (\tau_x, \tau_y, \tau_z)$ is a vector of Pauli matrices in the two-dimensional orbital basis. In this case the quantum metrics of the two bands are equal to each other, i.e., $g_{ij}^{+, \mathbf{k}} = g_{ij}^{-, \mathbf{k}}$, given that $g_{ij}^{s\mathbf{k}} = 2\text{Re}\langle \partial_i s_{\mathbf{k}} | (-s)_{\mathbf{k}} \rangle \langle (-s)_{\mathbf{k}} | \partial_j s_{\mathbf{k}} \rangle$ and $\sum_{s\mathbf{k}} |s_{\mathbf{k}}\rangle \langle s_{\mathbf{k}}| = \mathcal{I}_2$. For this reason Eq. (17) can be written as $\sum_{s\mathbf{k}} g_{ij}^{s\mathbf{k}} / (2d_0^{\mathbf{k}} - E_b)$, leading to $(M_{\text{inter}}^{-1})_{ij} = -\frac{2}{D} \sum_{s\mathbf{k}} \frac{s d_{\mathbf{k}} g_{ij}^{s\mathbf{k}}}{(2\varepsilon_{s\mathbf{k}} - E_b)(2d_0^{\mathbf{k}} - E_b)}$. These are again in full agreement with the literature [18].

Lastly we apply Eqs. (14)–(17) to the kagome lattice and solve them self-consistently for E_b and M_b . Their numerical values are presented, respectively, in Figs. 3(b) and 3(c) as a function of U . In this particular case \mathbf{M}_b is an isotropic matrix

with $(M_b^{-1})_{ij} = \delta_{ij}/M_b$. We find that while $E_b = -4|t| - U/3$ increases linearly in the small- U limit due to the presence of a flat lower band in a three-band lattice, $E_b = -U$ in the large- U limit which is similar to what happens in a one-band lattice. Similarly while $M_b = r_1/[a^2 U \ln(r_2|t|/U)]$ diverges logarithmically in the small- U limit due to the presence of a band touching with a nonisolated flat band, $M_b = U/(a^2 t^2)$ increases linearly in the large- U limit, which is again similar to what happens in a one-band lattice. Here r_1 and r_2 are real positive constants. In comparison, in the absence of a band touching (i.e., for an isolated flat band), we note that $M_b = r_3/(a^2 U)$ diverges with a power law in the small- U limit [17]. Furthermore we find that $E_b \approx -4.934|t|$ and $M_b \approx 12.574/(|t|a^2)$ when $U = 2|t|$, and they provide a perfect fit for the exact results in the small- q limit. This is shown in Fig. 3(a).

We note in passing that $1/M_b^{\text{inter},1} > 0$ is in direct competition with $1/M_b^{\text{inter},2} < 0$, and their magnitudes are about 3 orders of magnitude larger than $1/M_b^{\text{intra}}$. However, their sum $1/M_b^{\text{inter}} = 1/M_b^{\text{inter},1} + 1/M_b^{\text{inter},2}$ is quite comparable to $1/M_b^{\text{intra}}$ as can be seen in Fig. 3(c). Having shown that Eqs. (15)–(17) are exact for the kagome lattice for all U values, next we discuss their versatility for other lattices.

IV. SPATIALLY UNIFORM PAIRING

In accordance with the analysis presented above, Eqs. (15)–(17) are clearly exact for those multiband lattices that simultaneously fulfill the following conditions: (i) the Bloch Hamiltonian must exhibit time-reversal symmetry and (ii) the resultant two-body wave function must have a uniform contribution from all of the underlying sublattices. The latter is the so-called spatially uniform-pairing condition, and it is expected to be satisfied by those Bloch Hamiltonians that are invariant under the interchange of their sublattices. Note that if condition (ii) is satisfied for the two-body problem in a lattice then we expect the mean-field pairing order parameter ($\Delta_{S_i} = \Delta_S$) for the many-body problem to be spatially uniform; i.e., $\Delta_S = \Delta$ is equal for all of the sublattices.

In the case of two-band lattices while the honeycomb, Mielke checkerboard, Kane-Mele, Creutz and Haldane type Hubbard models with on-site interactions are among those popular lattices that satisfy condition (ii), i.e., because of their inversion symmetry, the sawtooth and zigzag type models are not. Here we note that the time-reversal symmetry is broken for the Creutz and Haldane models. In the case of three-band lattices, while the kagome lattice with on-site interaction satisfies condition (ii), the Lieb and dice lattices do not, since only two of their sublattices are interchangeable with each other but not the third one. According to the recent findings [11,17], the contribution to the two-body wave function from the noninterchangeable sublattice vanishes for both of these models in the small- U limit. Because of this, Eqs. (15)–(17) still work for these models but only in the $U/t \rightarrow 0$ limit. In particular, since the flat band of the Lieb lattice is isolated from the other bands with a gap, it is sufficient to keep only the flat-band contribution coming from Eq. (16) in the small- U limit. However, since the flat band of the dice lattice is in touch with one of the dispersive bands, one needs to keep both the

flat-band contribution and that of the touching band coming from Eqs. (15)–(17) in the small- U limit.

V. CONCLUSION

To summarize, here we considered an on-site attraction U between a spin- \uparrow and a spin- \downarrow fermion in a multiband lattice and derived an exact relation between the inverse of the effective-mass tensor $(M_b^{-1})_{ij}$ of the lowest bound states E_{1q} and the quantum-metric tensor g_{ij}^{nk} of the underlying Bloch states $|n_{\mathbf{k}}\rangle$. In addition to the intraband contribution $(M_{\text{intra}}^{-1})_{ij}$ that depends only on the single-particle spectrum $\varepsilon_{n\mathbf{k}}$ and the interband contribution $(M_{\text{inter},1}^{-1})_{ij}$ that is controlled by g_{ij}^{nk} , our generalized relation has an additional interband contribution $(M_{\text{inter},2}^{-1})_{ij}$ that depends on the band-resolved quantum metric g_{ij}^{nmk} . Our analytical expression is applicable to those multiband lattices that simultaneously exhibit time-reversal symmetry and fulfill the condition on spatially uniform pairing. It reproduces the previously known results including

that of isolated flat bands in the small- U limit [17] and that of two-band lattices for arbitrary U [18]. Furthermore, we also solved the two-body problem in a kagome lattice with nearest-neighbor hoppings and showed that the exact relation provides a perfect benchmark for this three-band lattice. In general, it is probably not possible to isolate the geometric contributions to the effective mass and study their effects alone in the experiments. However, our results for a flat band show that the geometric contributions play a dominant role in the small- U limit and can be studied there. As an outlook, our exact relation may find direct applications in many other lattices including those of the moiré materials [29], motivated by the hope that the formation of a two-body bound state can be used as a precursor to superconductivity in these systems.

ACKNOWLEDGMENT

The author acknowledges funding from TÜBİTAK Grant No. 1001-118F359.

-
- [1] J. P. Provost and G. Vallee, Riemannian structure on manifolds of quantum states, *Commun. Math. Phys.* **76**, 289 (1980).
- [2] M. V. Berry, The quantum phase, five years after, in *Geometric Phases in Physics*, edited by A. Shapere and F. Wilczek (World Scientific, Singapore, 1989).
- [3] R. Resta, The insulating state of matter: A geometrical theory, *Eur. Phys. J. B* **79**, 121 (2011).
- [4] S. Peotta and P. Törmä, Superfluidity in topologically nontrivial flat bands, *Nat. Commun.* **6**, 8944 (2015).
- [5] A. Julku, S. Peotta, T. I. Vanhala, D.-H. Kim, and P. Törmä, Geometric Origin of Superfluidity in the Lieb-Lattice Flat Band, *Phys. Rev. Lett.* **117**, 045303 (2016).
- [6] L. Liang, T. I. Vanhala, S. Peotta, T. Siro, A. Harju, and P. Törmä, Band geometry, Berry curvature, and superfluid weight, *Phys. Rev. B* **95**, 024515 (2017).
- [7] M. Iskin, Quantum metric contribution to the pair mass in spin-orbit-coupled Fermi superfluids, *Phys. Rev. A* **97**, 033625 (2018).
- [8] M. Iskin, Origin of flat-band superfluidity on the Mielke checkerboard lattice, *Phys. Rev. A* **99**, 053608 (2019).
- [9] Z. Wang, G. Chaudhary, Q. Chen, and K. Levin, Quantum geometric contributions to the BKT transition: Beyond mean field theory, *Phys. Rev. B* **102**, 184504 (2020).
- [10] M. Iskin, Collective excitations of a BCS superfluid in the presence of two sublattices, *Phys. Rev. A* **101**, 053631 (2020).
- [11] Y.-R. Wu, X.-F. Zhang, C.-F. Liu, W.-M. Liu, and Y.-C. Zhang, Superfluid density and collective modes of fermion superfluid in dice lattice, *Sci. Rep.* **11**, 13572 (2021).
- [12] L. Asteria, D. T. Tran, T. Ozawa, M. Tarnowski, B. S. Rem, N. Fläschner, K. Sengstock, N. Goldman, and C. Weitenberg, Measuring quantized circular dichroism in ultracold topological matter, *Nat. Phys.* **15**, 449 (2019).
- [13] M. Yu, P. Yang, M. Gong, Q. Cao, Q. Lu, H. Liu, S. Zhang, M. B. Plenio, F. Jelezko, T. Ozawa, N. Goldman, S. Zhang, and J. Cai, Experimental measurement of the quantum geometric tensor using coupled qubits in diamond, *Natl. Sci. Rev.* **7**, 254 (2020).
- [14] A. Gianfrate, O. Bleu, L. Dominici, V. Ardizzone, M. De Giorgi, D. Ballarini, G. Lerario, K. West, L. Pfeiffer, D. Solnyshkov, D. Sanvitto, and G. Malpuech, Measurement of the quantum geometric tensor and of the anomalous Hall drift, *Nature (London)* **578**, 381 (2020).
- [15] X. Tan, D.-W. Zhang, Z. Yang, J. Chu, Y.-Q. Zhu, D. Li, X. Yang, S. Song, Z. Han, Z. Li, Y. Dong, H.-F. Yu, H. Yan, S.-L. Zhu, and Y. Yu, Experimental Measurement of the Quantum Metric Tensor and Related Topological Phase Transition with a Superconducting Qubit, *Phys. Rev. Lett.* **122**, 210401 (2019).
- [16] Q. Liao, C. Leblanc, J. Ren, F. Li, Y. Li, D. Solnyshkov, G. Malpuech, J. Yao, and H. Fu, Experimental Measurement of the Divergent Quantum Metric of an Exceptional Point, *Phys. Rev. Lett.* **127**, 107402 (2021).
- [17] P. Törmä, L. Liang, and S. Peotta, Quantum metric and effective mass of a two-body bound state in a flat band, *Phys. Rev. B* **98**, 220511(R) (2018).
- [18] M. Iskin, Two-body problem in a multiband lattice and the role of quantum geometry, *Phys. Rev. A* **103**, 053311 (2021).
- [19] G.-B. Jo, J. Guzman, C. K. Thomas, P. Hosur, A. Vishwanath, and D. M. Stamper-Kurn, Ultracold Atoms in a Tunable Optical Kagome Lattice, *Phys. Rev. Lett.* **108**, 045305 (2012).
- [20] Y. Nakata, T. Okada, T. Nakanishi, and M. Kitano, Observation of flat band for terahertz spoof plasmons in a metallic Kagome lattice, *Phys. Rev. B* **85**, 205128 (2012).
- [21] Z. Li, J. Zhuang, L. Wang, H. Feng, Q. Gao, X. Xu, W. Hao, X. Wang, C. Zhang, K. Wu, S. X. Dou, L. Chen, Z. Hu, and Y. Du, Realization of flat band with possible nontrivial topology in electronic Kagome lattice, *Sci. Adv.* **4**, eaau4511 (2018).
- [22] T.-H. Leung, M. N. Schwarz, S.-W. Chang, C. D. Brown, G. Unnikrishnan, and D. Stamper-Kurn, Interaction-Enhanced Group Velocity of Bosons in the Flat Band of an Optical Kagome Lattice, *Phys. Rev. Lett.* **125**, 133001 (2020).
- [23] F. Diebel, D. Leykam, S. Kroesen, C. Denz, and A. S. Desyatnikov, Conical Diffraction and Composite Lieb Bosons in Photonic Lattices, *Phys. Rev. Lett.* **116**, 183902 (2016).

- [24] S. Kajiwara, Y. Urade, Y. Nakata, T. Nakanishi, and M. Kitano, Observation of a nonradiative flat band for spoof surface plasmons in a metallic Lieb lattice, *Phys. Rev. B* **93**, 075126 (2016).
- [25] H. Ozawa, S. Taie, T. Ichinose, and Y. Takahashi, Interaction-Driven Shift and Distortion of a Flat Band in an Optical Lieb Lattice, *Phys. Rev. Lett.* **118**, 175301 (2017).
- [26] C. Barreteau, F. Ducastelle, and T. Mallah, A bird's eye view on the flat and conic band world of the honeycomb and Kagome lattices: towards an understanding of 2D metal-organic frameworks electronic structure, *J. Phys.: Condens. Matter* **29**, 465302 (2017).
- [27] T. Mizoguchi and M. Udagawa, Flat-band engineering in tight-binding models: Beyond the nearest-neighbor hopping, *Phys. Rev. B* **99**, 235118 (2019).
- [28] In the case of two-band lattices there are two distinct branches in the two-body spectrum. Assuming on-site attraction and uniform pairing, it can be shown that the lower (upper) branch is associated with the Goldstone (Leggett) modes that describe the perfectly in-phase (out-of-phase) collective fluctuations of the superfluid order parameter on two different sublattices [18]. For this reason $\beta_{1\mathbf{q}} \propto (1, 1)$ is a manifestation of the perfectly in-phase sublattice contribution to the pair formation.
- [29] G. E. Topp, C. J. Eckhardt, D. M. Kennes, M. A. Sentef, and P. Törmä, Light-matter coupling and quantum geometry in moiré materials, *Phys. Rev. B* **104**, 064306 (2021).

Correction: Equation (10) contained a minor error and has been fixed.